The influence of hydrogen molecules on shock-cloud collisions

A. Horváth[1] and U. Ziegler[2]

[1] Széchenyi István College, Department of Mathematics, Hédervári u. 3., H-9026 Győr, and Loránd Eötvös University, Budapest, Hungary
[2] Institut für Theoretische Astrophysik der Universität Heidelberg, Tiergartenstrasse 15, D-69121 Heidelberg, Germany

Abstract. The interaction of shock fronts with molecular clouds is investigated. For this purpose, a two-fluid model describing an H–H_2 gas mixture is applied. The resulting equations are solved with a 2D axial-symmetric, fully compressive hydrodynamics code. Radiative cooling and the thermodynamical properties of the H_2 molecule, ie. rotational and vibrational degrees of freedom as well as thermal dissociation, are taken into account.

The evolution of the shock/cloud system using this more sophisticated thermodynamical model is found to be very different from that involving a pure atomic H gas which obeys the ideal gas law. For example, the maximum density of the shocked cloud is about 5–10 times lower in the latter case. This significant result might become very important when estimating triggered star formation rates. Another difference is that in the case of H-H_2 mixture, the shocked cloud gets a comet-like structure because of a smaller reexpansion.

From the numerical experiments we conclude that the application of the ideal gas law is insufficient and gives only a crude approximation of the real dynamics of a shock/cloud collision.

Key words: hydrodynamics – molecular data – methods: numerical – ISM: clouds

1. Introduction

The interstellar medium (ISM) is largely inhomogeneous as a result of supernova-explosions, ionisation fronts, and stellar winds from massive O or B stars steadily transferring energy into the ISM and keeping it in a turbulent state. The gas of the ISM can roughly be described by a three-phase model as mentioned by McKee & Ostriker (1977). Observations and theoretical calculations suggest that the hot rarefied bubbles of supernova remnants (SNRs) fill a significant part (40–60%) of the volume of the galactic disk (Tóth et al. (1996)). Heathcote & Brand (1983) argued that almost every small gas cloud in the galactic disk meets in its life with a shock front of a SNR. If this happens, the evolution of the molecular cloud is expected to be drastically altered.

Analytical work on shock/cloud collisions has been carried out by e.g. McKee & Cowie (1975), Spitzer (1982), Heathcote & Brand (1983) and McKee at al. (1987). The first hydrodynamical simulation has been presented by Sgro (1975). From that time on, numerical modeling of the dynamics of the shock/cloud interaction became a field of intense research (see e.g. Tenorio-Tagle & Rozicka (1986), Rozicka & Tenorio-Tagle (1987), Bedogni & Woodward (1992)). An excellent overview of the topic can be found in Klein et al. (1994). Numerical models showed a great progress in some respects. For example, there was a significant impovement in numerical techniques from the '70 s until now. Modern hydrodynamics codes are characterized by a higher degree of accuracy and less numerical diffusion, thus, producing much more accurate results at comparable grid resolution than the first codes did twenty years ago. The computing capacity shows a few orders of magnitude growth in the last two decades, too. This improvement made it possible to construct even 3D models including magnetic fields and radiative cooling processes at justifiable resolution. (See e.g. Stone & Norman (1992))

However, the majority of articles cited in the literature have one disadvantage in common: they use a very simple model for the ISM, ie. in most cases the ISM is assumed to be a pure atomic gas rather than a composition of several components. We present a two–fluid hydrodynamic model taking into account both H and H_2. Selfgravity and magnetic forces are ignored. The inclusion of these effects will be the subject of a future investigation. The neglect of selfgravity restricts our considerations to clouds with moderate mass. Albeit magnetic fields may influence the shock/cloud interaction, we will neglect them for the sake of simplicity. There is, however, one situation which justifies the neglect of magnetic forces: This is for high–latitude clouds far from the galactic midplane where the magnitude of the magnetic field has decreased to a value being dynamically unimportant. As a major aim of this paper, we will work out the differences arising from the use of a more complicated equation of state taking into account in more detail the thermodynamics of the H_2 molecule ie. rotational and vibrational excitation, and thermal dissociation, respectively. We assume cylindrical symmetry (2D model) and a cloud shape which is initially spherically symmetric.

The paper is organized as follows. In Sect. 2, we describe the thermodynamical model of the H-H$_2$ gas mixture. Sect. 3 briefly outlines the numerical method and the initial conditions. The results are presented in Sect. 4. We suggest a method which is hopefully adequate for the comparison of numerical results with observational data and show some radio maps of shocked clouds. Sect. 6 gives our conclusions.

2. The thermodynamical model

The interstellar medium is a mixture of different gas components. In the low temperature (non-ionized) region, the most important species are atomic and molecular hydrogen, and He. These three components contribute to about 99 percent of the interstellar mass.

An exact description of an H-H$_2$-He gas mixture requires a three-fluid numerical model and the solution of the equations for chemical reactions between the species. A three-fluid model, however, is very CPU time expensive. Because of the limited computer resources available, we consider only the two-fluid system consisting of H and H$_2$. The effects of He are omitted. We in addition assume that the only process leading to dissociation of H$_2$ results from thermal collisions. This is a valid assumption if there are no O or B stars nearby the cloud whose radiation field could dissociate H$_2$. We neglect the formation processes of H$_2$, because its time-scale is much longer than the considered time of interaction with the shock-front. Another argument for this assumption is that the shock front destroys the particles of interstellar dust which is the catalyst for H$_2$-formation. We also neglect ionisation processes. This reduces the applicability of our model: i.e. it is not valid when the temperature becomes higher than $\approx 10^4$ K.

In dense regions of molecular clouds, hydrogen is found in form of H$_2$. The dynamics of a H-H$_2$ gas mixture is quite different from that of an atomic gas. Let us assume a very cold dense H$_2$ gas. If this gas is heated by an outer source (i.e. compressional work) only a part of the gained thermal energy will fed into the kinetic energy of the particles. A significant fraction of the energy will be used for exciting rotational degrees of freedom and for the dissociation of H$_2$. For this reason, the pressure of the H-H$_2$ system will increase more slowly than the pressure of a H gas would do. It means for example, that the reexpansion of the shocked cloud will be smaller if we consider dissociation. We can state that using an appropriate model for the cloud/ISM system is important to get a realistic view of the shock-cloud interaction.

2.1. The equations of dynamical evolution

We assume that the two relevant gas species have the same fluid velocity and temperature. This is equivalent to the assumption of LTE. In this case the hydrodynamic equations we integrate read:

$$\frac{\partial \rho_H}{\partial t} + \mathrm{div}(\rho_H \boldsymbol{v}) = S_H(T, \rho_H, \rho_{H_2}) \tag{1}$$

$$\frac{\partial \rho_{H_2}}{\partial t} + \mathrm{div}(\rho_{H_2} \boldsymbol{v}) = S_{H_2}(T, \rho_H, \rho_{H_2}) \tag{2}$$

$$(\rho_H + \rho_{H_2})\left(\frac{\partial \boldsymbol{v}}{\partial t} + (\boldsymbol{v}\mathrm{grad})\boldsymbol{v}\right) = -\mathrm{grad}p \tag{3}$$

$$\frac{\partial u}{\partial t} + \boldsymbol{v}\mathrm{grad}u = -p\,\mathrm{div}\boldsymbol{v} + \Lambda(T, \rho_H, \rho_{H_2}) \tag{4}$$

The notations are as usual: ρ_H and ρ_{H_2} are the mass densities of H and H$_2$, T is the temperature, u is the energy density, p is the pressure, $\boldsymbol{v}$ is the velocity, Λ is the cooling function, S_H and S_{H_2} are the source terms of atomic and molecular hydrogen.

2.2. The energy density

In our model the energy density can be expressed as:

$$u(T) = \frac{kT}{m_H}\left(\frac{3}{2}\rho_H + \frac{f_2(T)}{4}\rho_{H_2}\right) + D_0\frac{\rho_H}{2m_H} \tag{5}$$

where $D_0 = 4.711$ eV is the dissociation energy of H$_2$, m_H is the mass of an H atom, and $f_2(T)$ is the degree of freedom for a H$_2$ molecule at temperature T. $f_2(T)$ can be written as:

$$f_2(T) = 3 + \frac{2}{kT}\left(f_{tot} + \frac{\Theta_v}{e^{\Theta_v/kT} - 1}\right) \tag{6}$$

where

$$f_{tot} = \frac{z_p f_p + 3z_o f_o}{z_p + 3z_o} \tag{7}$$

$$z_p = \sum_{j=0,2,4,\ldots}^{\infty} (2j+1)e^{-j(j+1)\Theta_r/T} \tag{8}$$

$$z_o = \sum_{j=1,3,5,\ldots}^{\infty} (2j+1)e^{-j(j+1)\Theta_r/T} \tag{9}$$

$$f_p = T^2\frac{\partial \ln z_p}{\partial T} \tag{10}$$

$$f_o = T^2\frac{\partial \ln z_o}{\partial T} \tag{11}$$

Here $\Theta_v = 6100$ K and $\Theta_r = 85.4$ K.

Because it is very expensive to calculate the above formulas, we use large interpolation arrays for their evaluation. These arrays are computed only once at the beginning of every computational run.

2.3. The equation of state

The total pressure can be expressed as:

$$p = \frac{kT}{m_H}\left(\rho_H + \frac{\rho_{H_2}}{2}\right) \tag{12}$$

We use this equation of state in combination with Eq. (5) to get the temperature as a function of energy density. To demostrate the difference between this equation of state and the equation of state of an ideal gas we plot the pressure as a function of energy density at $\rho_H = 0$, $\rho_{H_2} = 1\,m_H/\mathrm{cm}^3$, from $T_{min} = 20$ K to $T_{max} = 200$ K. It is shown in Fig. 1.
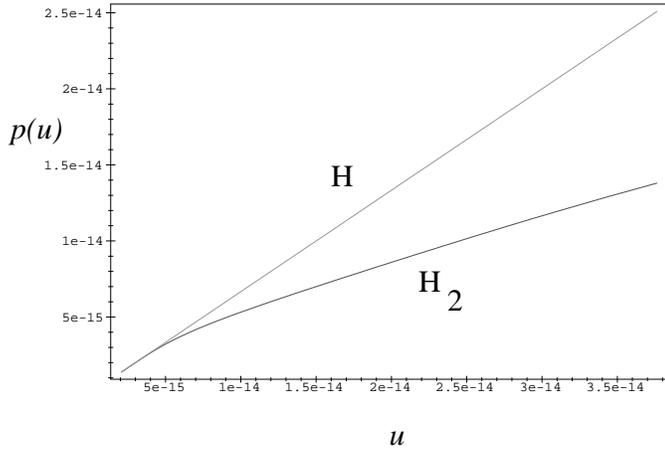
Fig. 1. The pressure of the H and H_2-gas as a function of energy density. See text for more details.

One can clearly see that the pressure of the molecular gas grows more slowly than the pressure of ideal atomic gas as a function of the energy density. It means that the molecular gas is much more compressible than the atomic one. The differences in this temperature domain are due to the possibility of excitation of rotational and vibrational degrees of freedom of H_2. At approximately 1000 K dissociation becomes important and it has a similar effect, i.e. the pressure will grow slowly with the energy density, but this process can not be described with a simple equation of state like in the low temperature domain.

We have to note that we assumed the rotational levels of the H_2 to be populated according to the thermal equilibrium. An exact numerical model should not use this assummption but calculate the population of the rotational levels and the excitational processes during the numerical calculation.

The assumption is valid in the predominant part of the integration domain in our model, because the typical elementary timestep is 10^{10}–10^{11} s, the typical density in H_2-regions is 10^2–10^3 cm^{-3}. According to Flower (1998) the typical rate coefficients of rotational transitions are in the order of 10^{-11}–10^{-13} cm^3 s^{-1} at temperatures more or equal than 150 K, which means that at these temperatures the characteristic time of the rotational transitions are less than the elementary timestep of our calculations. The assumption of the thermal equilibrium is not valid for the rotational levels at temperatures between 60 and 150 K.

The difference between the energy density of H_2 with and without rotational levels is 20% at 80 K, 35% at 100 K and 50% at 150 K. This way the inaccuracy of our assumption is in this magnitude at this temperature domain depending on the speed of changing of the temperature. Below 60 K the effect of the rotational levels is less than 10%, over 150 K then rate coefficients of rotational transitions are high enough. We can conclude that the inaccuracy of our equilibrium model arises in a small temperature domain and the relative error is in the order of 50% in the worst case. The effect of this inaccuracy is probably not important in our dynamical model, because the predominant part of the molecular cloud is out of this temperature domain. Surely,

this model is much more accurate than the usual ones with ideal gas dynamics.

We can state that an exact model with the calculation of rotational level would make small changes in the dynamics but it would require much more CPU-cost. Hence we assumed the rotational levels to be populated according to the thermal equilibrium.

2.4. The cooling function

Radiative cooling plays an important role in the processes examined in our calculations. At moderate densities we can use the optically thin approximation. We adopt the same cooling function as in Monaghan & Lattanzio (1989), except that we use a heating part proportional to the total density. The cooling function itself is a very extended formula, so we dispense with writing it.

2.5. The source terms

We use the source terms (S_H and S_{H_2}) for the calculation of dissociational processes of Biro & Raga (1994) and Dove & Mandy (1986).

3. The numerical model

We use a modified version of an explicit hydrodynamics code originally developed by Ziegler (1995) (see also Stone & Norman ZEUS, 1992) to solve the equations in Sect. 2.1. The numerical method is based on splitting the system into smaller parts by operator-splitting: The advective terms are solved by a MUSCL-type scheme with monotonic central-difference slope limiter, the other terms are solved by explicit or implicit differencing schemes depending on the time-scales of the different processes. I.e. we solve the part according to H_2 dissociation with an implicit scheme, but apply a simple explicit method for the grad$p$ term. The method for the cooling term is discussed in a separate subsection.

We assume the molecular cloud to be spherically symmetric initially with uniform density and in pressure equilibrium with the surrounding homogeneous interstellar medium. A plane–parallel shock front is setup with the help of the Rankine–Huginot conditions for an atomic gas. Their application is valid, because in the homogeneous surroundings of the cloud the temperature is more than 1000 K. Thus we do not have H_2 molecules there. A graphical illustration of the initial configuration is shown in Fig. 2.

To follow the motion of the cloud, the computational grid is allowed to move i.e. we check the location of the cloud and shift the integration domain by one cell to keep the "head" of the cloud in the first third part of the integration domain. This is very important in our study, because, without this shifting, the tail of the shocked cloud would leave the integration domain and mass would be lost.

We use at most 640×240 spatial resolution in our calculations. Although Klein et al. (1994) suggests higher resolution to
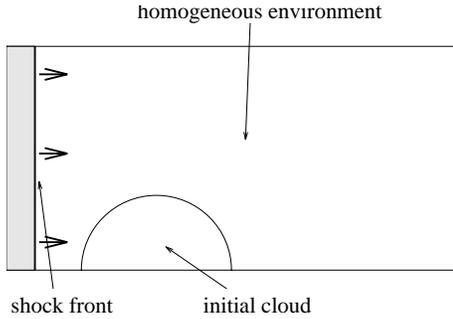
Fig. 2. Schematic picture of the initial configuration

resolve small-scale structures, we found that this resolution is enough to get the global structure of the cloud. (See the section "Results".)

The numerical simulations were performed on several workstations. (Namely on DEC Alpha/Digital Unix, IBM PC/Linux, and Sun/Solaris machines.)

3.1. The cooling routine

The characteristic time of the cooling processes is much smaller than the dynamical time-scales. In other words, the cooling term in the HD equations is a stiff term, and must be solved carefully adopting a stable numerical method. A common method is the Cranck-Nicholson scheme (CN) which needs to solve a nonlinear equation. It has the effect, that the calculation of the cooling term is CPU time consuming.

Here, we suggest a different method which we found to be ≈ 5 times faster than iterative methods reaching the same precision. We can write the stiff term in the following form:

$$\frac{du}{dt} = \Lambda(u, \rho_{\mathrm{H}}, \rho_{\mathrm{H}_2}) \tag{13}$$

At the beginning of the time-step we have a u_i value for the energy density and we want to get the new value u_{i+1} after a time–step Δt. The idea is to interpolate the function Λ with a linear function between the energy density at the beginning of time-step and the equilibrium value. The linearized differential equation is analytically solvable. This way we get the following solution:

$$u_{i+1} = u_e + (u_i - u_e)\exp\left(-\frac{\Lambda(u_i, \rho_{\mathrm{H}}, \rho_{\mathrm{H}_2})}{u_e - u_i}\Delta t\right) \tag{14}$$

where u_e is the energy density in the equilibrium, i.e. $\Lambda(u_e, \rho_{\mathrm{H}}, \rho_{\mathrm{H}_2}) = 0$.

This method has the very important property that the energy density tends to the equilibrium value if we rise the time-step to infinity, so it is stable for arbitrary large time-steps. On the other hand, it is an explicit method and therefore no iteration is needed which results in faster execution compared eg. to the Cranck-Nicholson scheme (Horváth & Kiss (1996), Horváth & Horváth (1998)).

To apply this method we must know the equilibrium energy densities as a function of ρ_{H} and ρ_{H_2}. For this function we construct an interpolation table which is computed only once at the beginning of the model calculation.

One can note that it is usually not a good idea to approximate the cooling function with a linear function. It is true, but the Cranck-Nicholson makes a more ragged approximation: it approximates the cooling function with a constant function, where the constant is the average of initial and final values of the cooling function. (See Horváth & Horváth (1998) for a detailed comparision of the numerical methods.)

It is important to note, that in our algorithm we split the two terms on the right hand side of (4). To decrease the error due to the splitting, we apply symmetric splitting, i.e. we make a half-time cooling step, then a full time step including the compressional work, and a half cooling step again. We can do it, because the cooling routine is fast, and this kind of splitting reduces the error by a factor of 10 in our calculations. The splitting method applied has a lot of good properties which are studied by mathematicians, see e.g. Horváth, Z. (1993).

4. Results

Although the HD code has been checked for a wide range of test problems, we made several test calculations to verify it. For example, we could reproduce the results of Bedogni & Woodward (1992) within a small difference if we set $\rho_{\mathrm{H}_2} = 0$ and switch off cooling.

The actual cloud/shock models are characterized by the following parameters which fix the physical conditions:

- ρ_{cl}: the central density of the cloud in units of $m_{\mathrm{H}}/\mathrm{cm}^3$.
- R_{cl}: radius of the cloud.
- T_{cl}: central temperature of the cloud.
- χ: density ratio. $\chi = \rho_{\mathrm{cl}}/\rho_{\mathrm{out}}$, where ρ_{out} is the density of the homogeneous environment.
- M: Mach-number of the shock front.

The initial state of the cloud is assumed to be homogeneous, $\rho_{\mathrm{H}} = 0$ at the center and $\rho_{\mathrm{H}_2} = 0$ outside. We set the temperature in a way to achieve pressure-equilibrium. The homogeneous initial conditions are necessary to achieve static initial state in our numerical model. However the pressure equilibrium could be achieved by an adequate distribuion of the temperature, the thermal equilibrium between the cooling and heating processes is not accesible in the framework of our model in a non homogeneous cloud.

The results of the numerical computations are visualized by density contour lines. In addition some global parameters, namely the position and velocity of the center of mass for different density regions are calculated. These regions are: (a) $\rho_{\mathrm{H}} + \rho_{\mathrm{H}_2} > 10 m_{\mathrm{H}}/\mathrm{cm}^3$, (b) $\rho_{\mathrm{H}} + \rho_{\mathrm{H}_2} > 100 m_{\mathrm{H}}/\mathrm{cm}^3$, (c) $\rho_{\mathrm{H}} + \rho_{\mathrm{H}_2} > 1000 m_{\mathrm{H}}/\mathrm{cm}^3$, and (d) $\rho_{\mathrm{H}} + \rho_{\mathrm{H}_2} > 10000 m_{\mathrm{H}}/\mathrm{cm}^3$.

The idea which lies behind this separation in density classes arises from our plan to compare the numerical results with radio– and infrared observations. These observations usually have 20–100 points inside the molecular clouds, so that at present only the global structure of a cloud can be mapped. Using observations of different lines it is possible to observe

the low-, medium- and high density components and to calculate the relative positions of their centers of mass. For example, in the lines of NH_3 we can observe the regions where $\rho > 10^4 m_H/cm^3$.

In the following graphical presentations the global parameters of type–(a) (type–(b), type–(c), type–(d)) region are shown as solid (dotted, dashed, dash-dotted) lines.

We also present the maximum densities as a function of time. We have to note, that it is only an informative parameter, because it depends on the resolution: higher resolution yields sharper shocks and higher densities. Nevertheless, it is an important indicator of the compression of the cloud.

4.1. The influence of dissociational processes

In this subsection we demonstrate that there arises a significant difference between the ideal gas model and our model. To illustrate it, we present here the results of two simulations adopting the same parameters. The difference between them is that in the first case we set $\rho_{H_2} = 0$, so we have a pure atomic H gas obeying the equation of state of an ideal gas.

The parameters are the following: $\rho_{cl} = 100\,m_H/cm^3$, $R_{cl} = 0.58\,pc$, $T_{cl} = 20\,K$, $\chi = 100$ and $M = 5$.

In this test calculations we neglect radiative cooling to focus only on the effects related to the presence of H_2 molecules. It is important to emphasize that in this case we just want to demonstrate the differences between simple H-dynamics and the dynamics of an H-H_2 gas mixture and not to give an accurate model of this process. The reason why we do not use radiative cooling in this test is that the cooling function of a pure H-gas and that of an H-H_2 mixture are different and we want to concentrate on the differences due to the thermodynamics of H_2.

The results are shown in Fig. 3. Both contour map series show the logarithm of total density at levels $\log(\rho_{tot}m_H^{-1}cm^3) = -1, 0, 1, 2, 3, 4, 5$.

In Fig. 4 we present the global parameters for two cases.

A significant difference between the two cases is observed. The main point is that in the case of the mixture a more compact and dense cloud core is built. This result is in good agreement with the theoretical expectations mentioned in Sect. 2. In the case of ideal gas dynamics the density-domain (d) does not appear. Another difference is that the cloud drag is smaller in the case of H-H_2-dynamics because of the smaller reexpansion.

Another difference is, that in the case of H-H_2 mixture the reexpansion is smaller, and thus a more significant part of the initial cloud will form a comet-like tail. In the case of ideal gas dynamics the tail has no such comet-like structure, while the observed shocked clouds show a long comet-like tail. It was a big discrepancy between the numerical tests and the observational data, and this problem was mentioned in Rozicka & Tenorio-Tagle (1987) and Klein et al. (1994) with no proposed solution.

Because the dynamics of a H-H_2 gas shows significant differences compared to the simple H gas, from now on, we show only the results of the H-H_2 mixture calculations.

Table 1. Global parameters at 320×120 resolution. The center ot mass and velocity of center of mass of different density regions are shown at $T = 3T_{ic}$ (X_3, V_3) and $T = 6T_{ic}$ (X_6, V_6). The units are 10^{18} cm and 10^5 cms^{-1} respectively.

	X_3	V_3	X_6	V_6
(a)	3.39	2.67	4.98	3.74
(b)	3.34	2.64	4.96	3.72
(c)	2.99	4.52	5.05	3.97
(d)	4.46	6.27	6.09	4.75

Table 2. Same as Table 1, however, with resolution 480×180.

	X_3	V_3	X_6	V_6
(a)	3.41	2.53	5.01	3.49
(b)	3.37	2.50	5.00	3.47
(c)	3.14	3.66	5.07	3.52
(d)	6.56	6.59	9.11	7.95

Table 3. Same as Table 1, however, with resolution 640×240.

|	X_3	V_3	X_6	V_6
(a)	3.46	2.34	5.01	3.42
(b)	3.42	2.28	5.02	3.40
(c)	3.25	3.94	5.05	3.38
(d)	4.56	4.72	5.95	4.68

4.2. Convergence test

In our calculations we used a 640×240 grid. It is very important to test whether this resolution is enough or not for our purposes. To check it, we performed a series of calculations with common parameters using different resolutions, namely 320×120, 480×180 and 640×240: $\rho_{cl} = 100\,m_H/cm^3$, $R_{cl} = 0.58\,pc$, $T_{cl} = 20\,K$, $\chi = 100$ and $M = 5$.

In Fig. 5, we show the global parameters and the density contour maps of $\log\rho_{H_2}$ of the calculations with different resolutions. In the Tables 1–3 we show the global quantities at $T = 4T_{ic}$ and $T = 8T_{ic}$ with the three different resolutions.

Fig. 5 shows, that the 640×240 resolution is enough for global parameters, because the positions and velocities of different density regions are almost the same at every resolution. It is especially valid for type–(a), type–(b) and type–(c) density regions. The difference of global parameters is less than 5% between the 640×240 and 480×180 cases in the position of center of mass and less than 10% in the velocity of center of mass.

The most remarkable difference arises in the case of type–(d) region (dot-dashed line). However, it is not really important, because there are only a few grid cells in the integration domain with density more than $10^4\,m_H/cm^3$ when $t < 6T_{ic}$, and this region takes only 1–2% of the total mass. (For example, with 320×120 resolution the (d) region contains less than 10 cell at $T = 3T_{ic}$.)

The density contour maps show similar global structures at the three resolutions, but the higher resolution give sharper edges and more small-scale details.
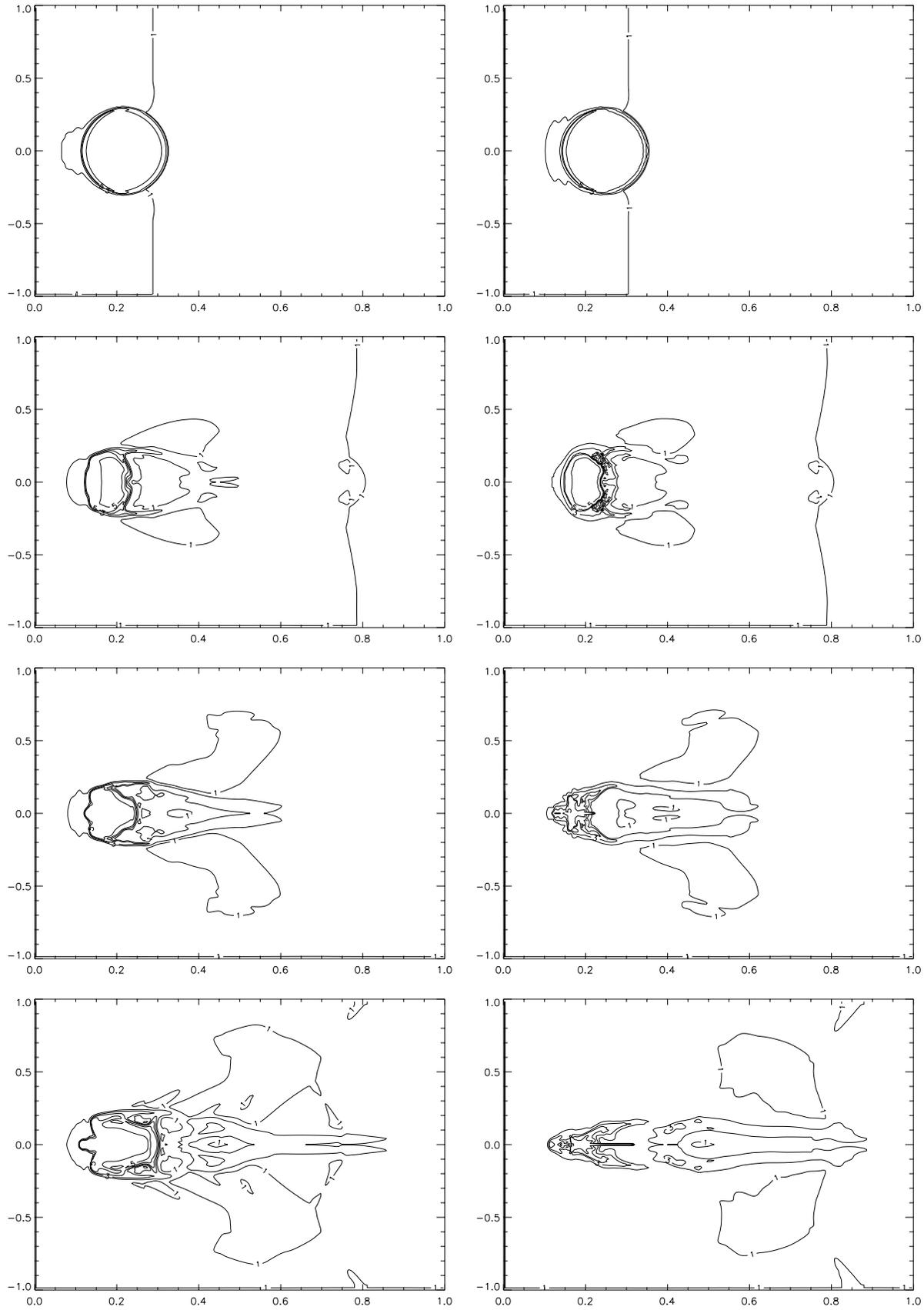
Fig. 3. Comparison of ideal gas dynamics (left side) and H-H$_2$ dynamics (right side). The time-step between frames is $2T_{ic}$. (See text for parameters)

Ideal gas dynamics

H-H$_2$-mixture
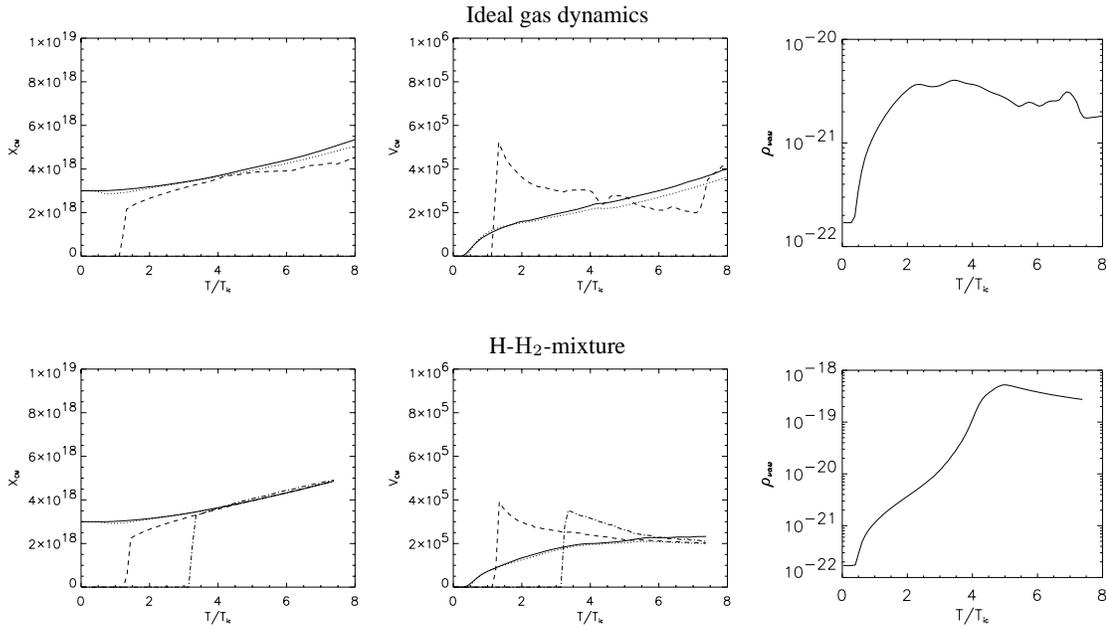
Fig. 4. Comparison of ideal gas dynamics and H-H$_2$ dynamics. The global parameters are plotted. The parameters are the same as in Fig. 3.

320×120
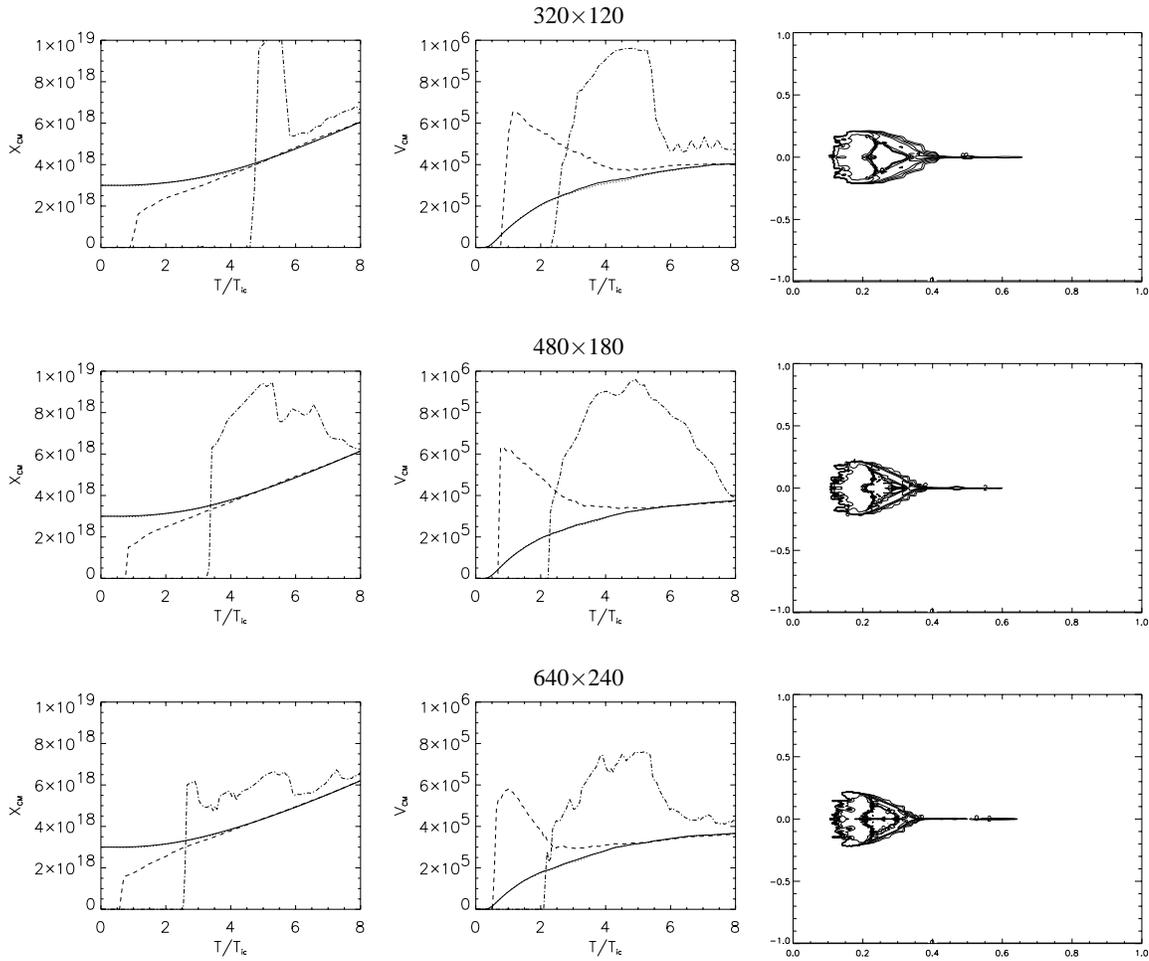
480×180

640×240

Fig. 5. A convergence test: Global parameters and H$_2$ density contour maps at $t = 5T_{ic}$ calculated on a 320×120, 480×180 and 640×240 grid using the same parameters. (See text.)
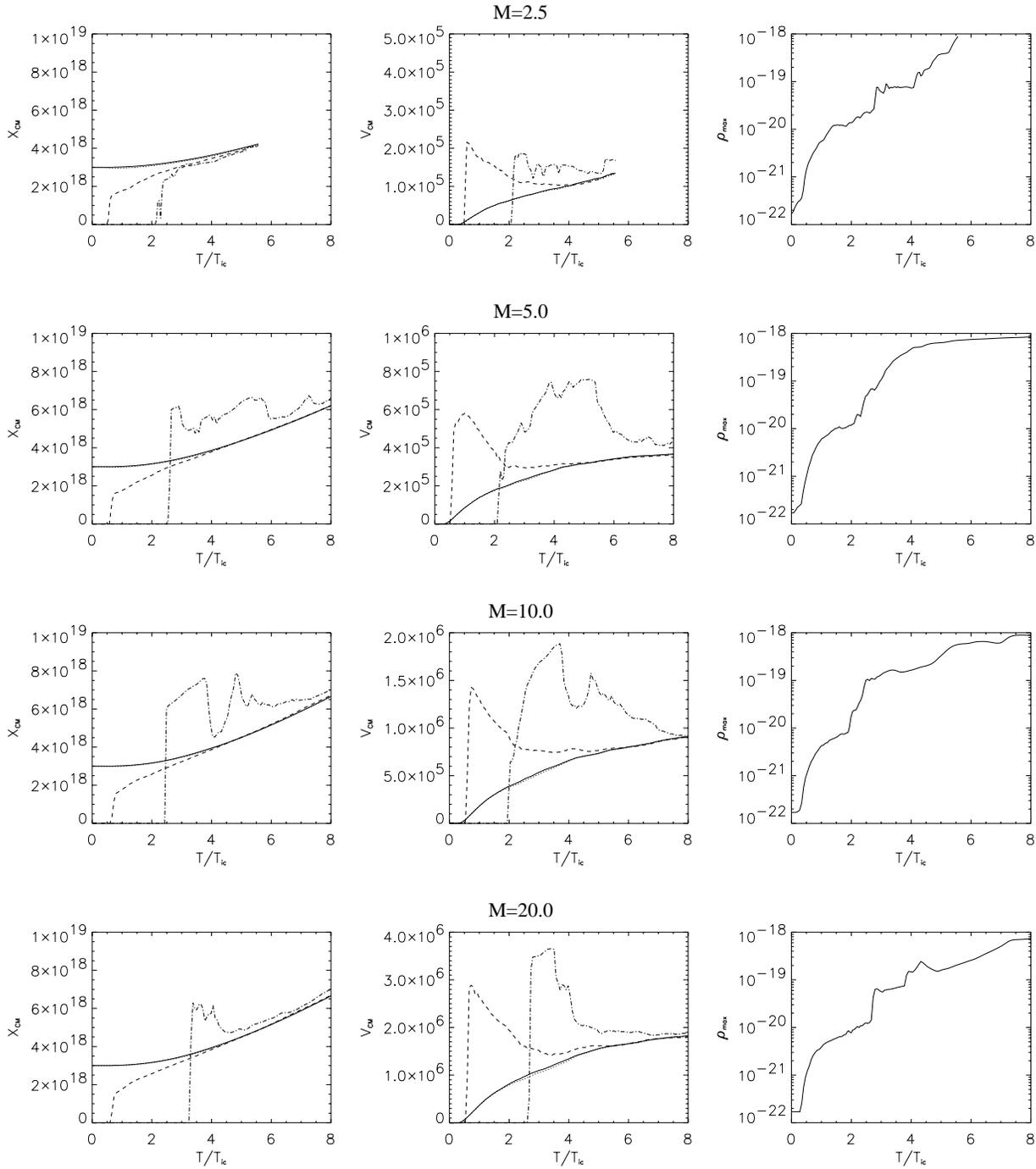
Fig. 6. Calculation with different Mach-numbers. See text for parameters.

We can summarize the results of the convergence test in the following two statements:

- The resolution 640×240 is enough to calculate the global structure of the cloud.
- The detailed study of small-scale processes needs higher resolution.

As we are mainly interested in the global structure of the shocked cloud, we can use the 640×240 resolution.

4.3. A series of models with different Mach-numbers

We also performed a series of calculations with different Mach-numbers. The other parameters are fixed: $\rho_{cl} = 100\,m_{\mathrm{H}}/\mathrm{cm}^3$, $R_{\mathrm{cl}} = 0.58\,\mathrm{pc}$, $T_{\mathrm{cl}} = 20\,\mathrm{K}$ and $\chi = 100$.

In Fig. 6, we present the main global quantities of the cloud for $M = 2.5, 5.0, 10.0, 20.0$.

It is important to note that the graphs of $M = 10$ and $M = 20$ cases are very similar. It means, that the Mach-scaling
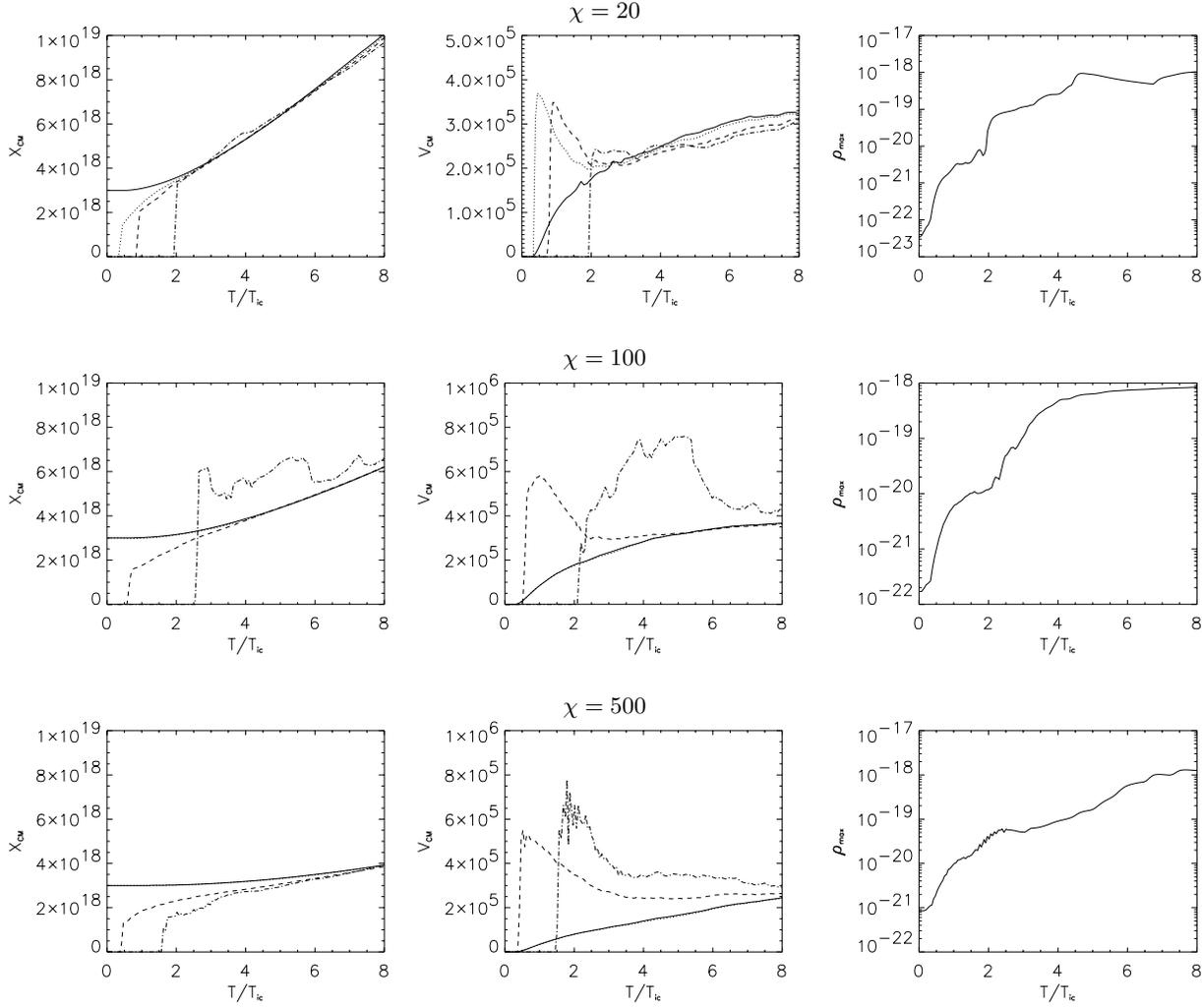
Fig. 7. Calculation with different central densities. See text for parameters.

(Klein et al., 1994) remains approximately true in the presence of dissociational processes and radiative cooling.

It is an important result, that the maximum density becomes lower when the Mach-number increases. The reason of it is, that in the case of fast shock there is less time for dissociational and radiative processes to operate. This way, the gas remains hot, and its pressure brakes the formation of high-density regions.

4.4. A series of models with different central densities

We also performed a series of calculations with different central densities with fixed density of the outer medium. The other parameters are as before: $\rho_{out} = 1 \, m_H/cm^3$, $R_{cl} = 0.58 \, pc$, $T_{cl} = 20 \, K$.

In Fig. 7, we present the main global quantities of the cloud for $\chi = 20.0, 100.0, 500.0$.

5. A qualititative comparision with observations

Finally, we note that the contour maps on Fig. 5 show a very similar structure like the observations of a shocked cloud in Tóth & Walmsley (1994), while we can not produce such a tail with ideal gas dynamics.

The main aspects of similarity are the following:

– The cloud has a dense head and a dense tail along the axis of symmetry.
– The outer part of the cloud overrun by the shock front forms a special shape: there is a cone-like structure between the head and the dense tail and the maximum density is reached at the surface of this cone.

This qualitative properties are well seen in the CO and NH_3 maps of L1251 cloud (Sato et al., 1994 and Tóth & Walmsley, 1994). Altougly, a precise numerical comparision of the observational results and our model needs an extended work with calculation of excitation of rotation levels of CO and NH_3 molecules, the qualitative similarities are prominent.

Contrary, with ideal gas dynamics we could not reproduce such a structure, because the dense tail along the axis and the cone-like structure did not appear. The reason is that in the ideal case the reexpansion is higher than in the case of H-H_2-mixture, and the outer parts of the cloud occupy a more extended volume.

6. Conclusions

We have constructed a numerical model for the simulation of the interaction between a shock front and a molecular cloud. In our two-fluid HD code we used a realistic thermodynamical description for a H-H_2 gas mixture, i.e. we took into account the rotational and vibrational degrees of freedom and thermal dissociation of H_2-molecules.

This new kind of modeling predicts a significant influence on the evolution of the shocked cloud. The main differences between atomic H and a H-H_2 mixture can be described shortly in three points:

- The maximum density during the interaction is much more higher if we take into account the rotational degrees of freedom and dissociational processes
- After the interaction we have a more compact and dense cloud than before the interaction
- The shocked cloud has a comet-like structure which is qualitatively similar to the observed sturctures in Tóth & Walmsley, while the models with ideal gas dynamics do not show such long tails

These differences are very important, and show that the more accurate thermodynamical description of the ISM is needed to get more realistic models of shock/cloud interaction.

We presented a few series of calculations with changing only one parameter. We could show that the Mach-scaling transformation remains approximately valid in our model.

In the next paper we will present a quantitative comparison of numerical and observational results.

References

Bedogni R., Woodward P.R., 1992, A&A 231, 481

Biro S., Raga A.C., 1994, ApJ 434, 221

Dove J.E., Mandy M.E., 1986, ApJ 311, L93

Flower D.R., 1998, MNRAS 297, 334

Heathcote S.R., Brand P.W.J.L., 1983, MNRAS 203, 67

Horváth A. Jr., Horváth Z., 1998, On fast numerical solution of special stiff equations arising in astrophysics. Annales Univ. Sci. Budapest., Sect. Comp., 1998, accepted for publication

Horváth A. Jr., Kiss Cs., 1996, Interstellar Shock-Cloud Collisions – New Methods For Cooling. In: Proceedings of The May Advanced School and Workshop on the Interaction of Stars with their Environment

Horváth Z., 1993, Consistency and stability for some nonnegativity conserving methods. Applied Numerical Mathematics 13, 371

Klein R.I., McKee C.F., Colella P., 1994, ApJ 420, 213

McKee C.F., Cowie L.L., 1975, ApJ 218, 148

McKee C.F., Ostriker S.R., 1977, ApJ 218, 148

McKee C.F., Hollenbach D.J., Seab C.G., Tielens A., 1987, ApJ 318, 674

Monaghan J.J., Lattanzio J.C., 1989, ApJS 41, 555

Rozicka M., Tenorio-Tagle G., 1987, A&A 176, 329

Sato F., Mizuno A., Nagahama T., et al., 1994, ApJ 435, 279

Sgro A.G., 1975, ApJ 197, 621

Spitzer L. Jr., 1982, ApJ 262, 315

Stone J.M., Norman M.L., 1992 ZEUS, ApJS 80, 753

Stone J.M., Norman M.L., 1992, ApJ 390, L17

Tenorio-Tagle G., Rozicka M., 1986, A&A 155, 120

Tóth L.V., Kiss Cs., Moór A., 1996, Catalogue of IRAS loops in the IInd Galactic quadrant. In: Käufl H.U. (ed.) The Role of Dust in the Formation of Stars. ESO Workshop, Garching, Germany, 1995. Springer, in press

Tóth L.V., Walmsley C.M., 1994, Water masers in L1251, IBVS 4107

Ziegler U., 1995, Ph.D. Thesis, University of Würzburg